# Revealing the Position Effect of an Alkylthio Side Chain in Phenyl-Substituted Benzodithiophene-Based Donor Polymers on the Photovoltaic Performance of Non-Fullerene Organic Solar Cells

Weichao Chen,[†,#] Gongyue Huang,[‡,#] Xiaoming Li,[‡] Yonghai Li,[‡] Huan Wang,[†] Huanxiang Jiang,[‡] Zhihui Zhao,*[†] Donghong Yu,*[∥,⊥] Ergang Wang,*[§] and Renqiang Yang*[‡]

[†]College of Textiles & Clothing, State Key Laboratory of Bio-Fibers and Eco-Textiles, Collaborative Innovation Center for Eco-Textiles of Shandong Province, Qingdao University, Qingdao 266071, China

[‡]CAS Key Laboratory of Bio-Based Materials, Qingdao Institute of Bioenergy and Bioprocess Technology, Chinese Academy of Sciences, Qingdao 266101, China

[§]Department of Chemistry and Chemical Engineering, Chalmers University of Technology, Göteborg SE-412 96, Sweden

[∥]Department of Chemistry and Bioscience, Aalborg University, Aalborg DK-9220, Denmark

[⊥]Sino-Danish Centre for Education and Research, Aarhus DK-8000, Denmark

✿ Supporting Information

**ABSTRACT:** In this work, position effects of an alkylthio side chain were investigated by designing and synthesizing two copolymers based on a phenyl-substituted benzo[1,2-$b$:4,5-$b'$]dithiophene (BDTP) and difluorobenzotriazole (FTAZ). The polymer based on the *meta*-position-alkylthiolated BDTP, named $m$-PBDTPS−FTAZ, showed a relatively broader bandgap (2.00 vs 1.96 eV) and lower highest occupied molecular orbital (HOMO) energy level (−5.40 vs −5.32 eV) than its *para*-positioned structural isomeric analogue polymer (named $p$-PBDTPS−FTAZ), that is, $m$- and $p$-PBDTPS−FTAZ with the side chain structured as ethylhexyl- in the phenyl unit and hexyldecyl- in the FTAZ moiety. When blended with ITIC, $m$-PBDTPS−FTAZ showed a comparable crystallinity but more uniform morphology compared to that of $p$-PBDTPS−FTAZ. A high power conversion efficiency of 13.16% was achieved for $m$-PBDTPS−FTAZ:ITIC devices with a high open circuit voltage ($V_{OC}$) of 0.95 V, which is higher than that of $p$-PBDTPS−FTAZ:ITIC devices (10.86%) with a $V_{OC}$ of 0.89 V. Therefore, $m$-BDTPS could be an effective donor unit to construct high-efficiency polymers due to its effectively decreased HOMO energy level of polymers while still maintaining good molecular stacking.

**KEYWORDS:** broad bandgap, conjugated polymers, polymer solar cells, position effects, side chains
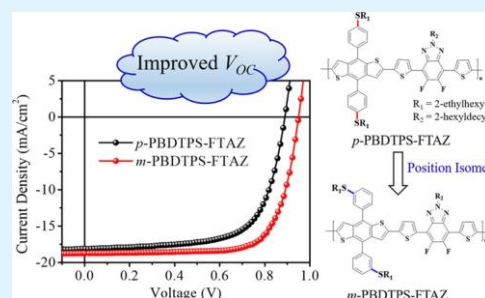
## INTRODUCTION

Organic solar cells (OSCs) have been considered as a promising photovoltaic technology for a bright marketing future due to its superiority in low cost, large-scale manufacture, flexibility, etc.[1−6] Based on the mutual development of photovoltaic materials and device-processing, remarkable progress has been achieved in the recent 2 years. Power-conversion efficiencies (PCEs) over 14−16% have been obtained for single-junction solar cells.[7−10] Particularly, a significant record PCE of 17.36% was reported by Chen et al. in tandem OSCs in 2018.[6] Therefore, PCEs of OSCs can be further improved through a series of rational material design and device-engineering. Photovoltaic materials, especially for donor materials, are always a hot research topic in the progress of OSCs.[11−22] Wide-bandgap (WBG) polymer donor materials among them acquired a remarkable breakthrough due to the rise of non-fullerene acceptor materials possessing a lower bandgap.[23−26] It is commonly known in the OSC community that the PCE is determined by three parameters, which are the short-circuit current density ($J_{SC}$), open-circuit voltage ($V_{OC}$), and fill factor (FF).[27] A large $J_{SC}$ depends on a broad absorption spectrum of photovoltaic materials, and a high $V_{OC}$ relies on an enlarged gap between the highest occupied molecular orbital (HOMO) energy levels of donors and the lowest unoccupied molecular orbital (LUMO) energy levels of acceptors. Therefore, a high-quality WBG donor material should possess a complementary absorption spectrum for a larger $J_{SC}$ and a lowered HOMO energy level for a higher $V_{OC}$, respectively.

Side-chain engineering, as an effective strategy, has been widely used for tuning the absorption spectra and energy levels of conjugated polymers. Benzo[1,2-$b$:4,5-$b'$]dithiophene (BDT) is a typical electron-donor unit for constructing high-efficiency donor materials because of the symmetrical and

planar molecular structure.[28,29] Its two-dimensional (2D) side chains and substitutents play an important role in tuning the energy level and absorption spectra of materials.[30−34] On the one hand, thienyl and phenyl as two main 2D groups have been studied. Compared with thienyl-substituted BDT (BDTT), phenyl-substituted BDT (BDTP) usually showed a weaker electron-donating effect due to its larger π-conjugated area and better planarity.[35−39] Therefore, BDTP-based donor materials usually showed lower HOMO levels and higher $V_{OC}$ values compared to BDTT-based materials. On the other hand, an alkylthio side chain was usually introduced into the BDT moiety for a high $V_{OC}$ as Li et al. reported in their pioneer work on alkylthiolation on the BDT type of donor materials.[40] Therefore, alkylthio-phenyl-substituted BDT (BDTPS)-based donor materials presented a great performance with a high $V_{OC}$. However, these studies have been mainly concentrated on the *para*-position of the phenyl group (*p*-BDTPS) and alkylthiolation on other sites of the phenyl group has not been paid enough attention.[41] It is known that substitutents in different sites on the phenyl group could make a significant influence concerning the density distribution of electron clouds. When the phenyl group was alkylthiolated in its *meta*-position, the distance between the alkylthio group and the BDT core was shortened, which may improve the substituent group's conjugation effect and increase its π- electron-accommodating ability. In addition, its electron- withdrawing inductive effect might make a difference due to the closer distance in comparison with that of its analogue in the *para*-position. Therefore, it is crucial to investigate the position effect of an alkylthio-substituted side chain by molecular design strategies.

In this work, *m*-BDTPS and *p*-BDTPS as donor units were applied for the syntheses of two polymers with difluorobenzotriazole (FTAZ) as the acceptor unit, named *m*-PBDTPS−FTAZ and *p*-PBDTPS−FTAZ, respectively. Their chemical structures are illustrated in Figure 1a. The detailed synthetic

routes and structural characterizations are given in the Supporting Information. The polymer *m*-PBDTPS−FTAZ revealed a blue-shifted absorption spectrum and a lower HOMO energy level compared with *p*-PBDTPS−FTAZ due to the position-sensitive alkylthio-substituted side chain. Meanwhile, the position modification affects the molecular-packing distance (23.26 vs 20.26 Å for *p*-PBDTPS−FTAZ and *m*-PBDTPS−FTAZ, respectively), but has almost no effects on the crystallinity of the polymers. The corresponding solar cells based on *m*- and *p*-PBDTPS−FTAZ showed high PCEs over 10% with a large $J_{SC}$ (over 18 mA/cm$^2$). However, *m*-PBDTPS−FTAZ showed a higher PCE (13.16%) than *p*-PBDTPS−FTAZ:ITIC-based devices (10.86%), which mainly benefits from its higher $V_{OC}$ (0.95 vs 0.89 V) due to its lower HOMO level. More importantly, the high $V_{OC}$ indicated that *m*-PBDTPS−FTAZ would have a potentially increased PCE. Therefore, *m*-BDTPS could be used to construct high-performance polymer donors by carefully copolymerizing an appropriate acceptor unit to achieve a high $V_{OC}$ while maintaining a large $J_{SC}$ in OSCs from such *m*-BDTPS-based donor polymers.

## RESULTS AND DISCUSSION

The polymer *p*-PBDTPS−FTAZ and compound 1 were synthesized according to the literature.[37,41] The general synthetic routes of *m*-BDTPSSn and the corresponding polymers are shown in Scheme S1. $^1$H NMR and $^{13}$C NMR spectra were used to identify the chemical structure of the intermediates and final products. The polymer *m*-PBDTPS−FTAZ was synthesized by the Stille coupling reaction with $Pd_2(dba)_3/P(o\text{-tol})_3$ as the catalyst. The chemical structures of the two polymers are shown in Figure 1a. The detailed synthesis could be found in the Experiment Section of the Supporting Information. The two polymers displayed good solubility in general solvents such as chloroform (CF), chlorobenzene (CB), and *o*-dichlorobenzene (*o*-DCB), which was beneficial for fabricating photovoltaic devices through spin-coating. Their thermal properties were determined by thermogravimetric analysis (TGA). As shown in Figure S1, a good thermal stability was obtained for the two polymers with high onset decomposition temperature ($T_d$) values of 354 and 370 °C at 5% weight-loss for *p*- and *m*-PBDTPS−FTAZ, respectively. The *meta*-positioned alkylthio substituent on the side chain of BDT had a positive influence on the thermal ability of the material.

The UV−vis absorption spectra of the two polymers both in chloroform solutions and in neat films are shown in Figure 1b, and the obtained data are listed in Table 1. All of the four spectra showed two distinct absorption peaks between 450 and 650 nm. The main peak in the short wavelength was attributed to the intermolecular charge transfer, and the intense shoulder peak in the long wavelength implied that there should be a strong intra-/intermolecular aggregation. On the other hand, an apparent red shift was observed from solutions to their solid films, implying the intense intermolecular aggregation in


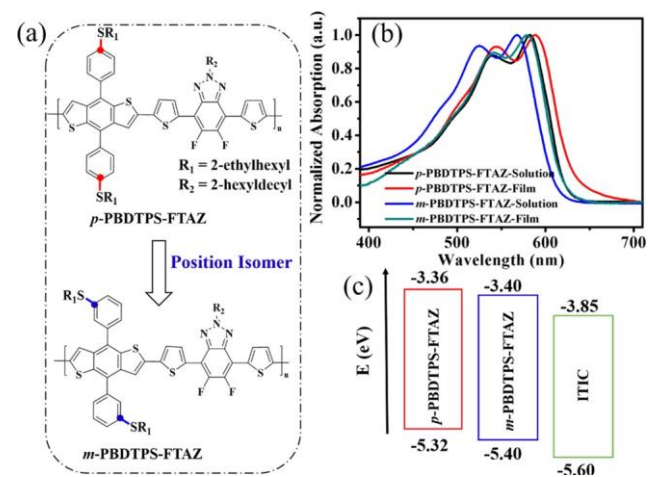
Figure 1. (a) Chemical structure, (b) normalized absorption spectra, and (c) energy level diagram of *m*- and *p*-PBDTPS−FTAZ and ITIC.

Table 1. Optical and Electrochemical Parameters of *m*- and *p*-PBDTPS−FTAZ

| polymer | $\lambda_{abs}$$^a$ (nm) | $\lambda_{onset}$$^a$ (nm) | $\lambda_{abs}$$^b$ (nm) | $\lambda_{onset}$$^b$ (nm) | $E_g^{opt}$ (eV) | $\varepsilon$ (M$^{-1}$cm$^{-1}$) | $E_{HOMO}$$^{CV}$ (eV) | $E_{LUMO}$$^c$ (eV) |
|---|---|---|---|---|---|---|---|---|
| *p*-PBDTPS−FTAZ | 540, 583 | 624 | 544, 589 | 633 | 1.96 | 0.62 × 10$^5$ | −5.32 | −3.36 |
| *m*-PBDTPS−FTAZ | 525, 567 | 612 | 542, 579 | 621 | 2.00 | 0.60 × 10$^5$ | −5.40 | −3.40 |

$^a$Measured in CF solution. $^b$Measured in the neat film. $^c$$E_{LUMO} = E_{HOMO}^{CV} + E_g^{opt}$.

pristine films. Nevertheless, compared with $p$-PBDTPS−FTAZ, $m$-PBDTPS−FTAZ exhibited a blue-shifted absorption spectrum. Their absorption edges in the films were 633 and 621 nm, respectively. The two polymers showed a similar molar extinction coefficient ($\varepsilon$) of about $0.6 \times 10^5 \, M^{-1} \, cm^{-1}$ (Table 1) in solution. Both polymers showed a favorable complementary absorption with ITIC, implying effective utilization of solar irradiation and a large $J_{SC}$. According to the empirical formula, the optical band gaps of $p$-PBDTPS−FTAZ and $m$-PBDTPS−FTAZ were respectively calculated to be 1.96 and 2.00 eV. It indicated that modulating the position of the alkylthio substitutents in polymer donor materials could be an effective strategy to adjust their optical properties.

Figure S2 shows cyclic voltammetry (CV) curves of $p$-PBDTPS−FTAZ and $m$-PBDTPS−FTAZ, and the corresponding data are listed in Table 1. Their energy-level diagrams are shown in Figure 1c. An onset oxidation potential of 0.93 V for the former and 1.01 V for the latter was observed. Based on the empirical formula, their HOMO energy levels were −5.32 and −5.40 eV, respectively. Their LUMO energy levels were calculated to be −3.36 and −3.40 eV by their HOMO energy levels and optical gaps. The $m$-positioned alkylthio substitutent on the phenyl group caused a decreased HOMO energy level by comparison with that of the $p$-positioned substitutent on the phenyl group. From the viewpoint of energy level, a decreased HOMO energy level was conducive to obtain a high $V_{OC}$.

The density functional theory (DFT) method was adopted for theoretical calculations at the B3LYP/6-31G level. To reduce the calculation workload, methyl groups were used to replace the long alkyl chains. HOMO energy levels were calculated for $p$- and $m$-BDTPS structural units (D) only. However, calculations on their molecular conformation were carried out on dimers of BDTPS and FTAZ (D−A). The HOMO energy level was lowered from −5.18 eV for $p$-BDTPS to −5.22 eV for $m$-BDTPS in terms of the donor unit as shown in Figure S3a. This result verified our design idea of regulating energy levels by changing different substituent sites. As shown in Figure S3b, a slightly larger torsion angle was observed for $m$-PBDTPS−FTAZ in comparison to that of the polymer $p$-PBDTPS−FTAZ. It may be caused by a larger steric hindrance of the $m$-substituent. Even so, they all exhibited a relatively plane backbone conformation, which could facilitate an effective interchain interaction and charge transport.

Single-junction OSCs were fabricated based on $p$- and $m$-PBDTPS−FTAZ as the donor materials and ITIC as the acceptor material. A typical device structure of indium-tin oxide (ITO)/poly(3,4-ethylenedioxythiophene):poly(styrene sulfonate) (PEDOT:PSS)/polymer:ITIC/PFN-Br/Al was adopted to test their photovoltaic performance. The $J$−$V$ curves under different ratios are given in Figure S4, and the optimal curves are given in Figure 2a. The detailed photovoltaic parameters are listed in Table 2. The thicknesses of the active layers were about 100−110 nm. $m$-PBDTPS−FTAZ showed an increased $V_{OC}$ of 0.95 V compared to 0.89 V in $p$-PBDTPS−FTAZ. The PCE was increased from 10.86% for $p$-PBDTPS−FTAZ to 13.16% for $m$-PBDTPS−FTAZ, which was mainly benefited by the higher $V_{OC}$ of the latter. In terms of the $V_{OC}$, the position of the alkylthio substituent on the phenyl side chain has a remarkable impact. This may be caused by the change of density distribution of electron clouds on the phenyl moiety. On the other hand, a slightly increased FF value for $m$-PBDTPS−FTAZ was obtained, which may be a
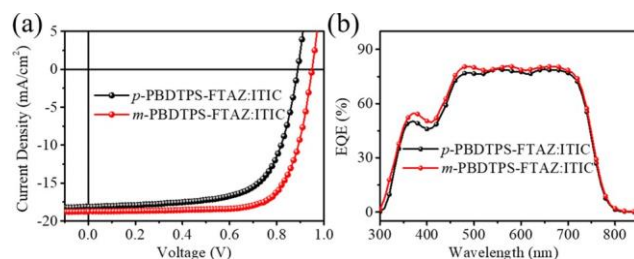


Figure 2. (a) $J$−$V$ curves and (b) external quantum efficiency (EQE) spectra of the optimized OSCs.

result of its more balanced charge-transport ability. Therefore, a promising BDT unit $m$-BDTPS was obtained for constructing polymers with a large $V_{OC}$ and FF under synergistic effects of the position of the substitute.

Based on the report from Bisquert and Garcia-Belmonte et al.,[42,43] we have performed a study on the chemical capacitance, enabling us to understand the relevant density of state (DOS), which determines the $V_{OC}$ of the devices. The chemical capacitance tests on $p$-PBDTPS−FTAZ:ITIC- and $m$-PBDTPS−FTAZ:ITIC-based OSC devices are displayed in Figure S5. A smaller downshift of the DOS of $m$-PBDTPS−FTAZ was found compared with that of $p$-PBDTPS−FTAZ. This may be one of the reasons for the higher $V_{OC}$ of $m$-PBDTPS−FTAZ:ITIC as the same acceptor ITIC was used.

As shown in Figure 2b, the OSCs based on both $p$- and $m$-PBDTPS−FTAZ showed a broad photoresponse during 350−750 nm. Particularly, a strong photoresponse ability was observed over 500−700 nm, which caused a large $J_{SC}$ of both OSCs (18.12 and 18.76 mA/cm$^2$ for $p$-PBDTPS−FTAZ and $m$-PBDTPS−FTAZ, respectively). The integrated current densities ($J_{SC}^{EQE}$) from the EQE curves were 17.51 and 18.15 mA/cm$^2$ for their OSCs, respectively, being consistent with the measured $J_{SC}$ values with an error <5%. The relatively higher $J_{SC}$ based on $m$-PBDTPS−FTAZ:ITIC may be benefited from the better morphologies as shown in Figure 3.

Blended-film morphologies were studied via the measurements of an atomic force microscope (AFM) and a transmission electron microscope (TEM). As shown in Figure 3a,b, both the optimal blend films showed relatively smooth surfaces with root mean square (RMS) surface roughnesses of 1.09 and 0.99 nm for $p$- and $m$-PBDTPS−FTAZ:ITIC blends, respectively. The $m$-PBDTPS−FTAZ:ITIC blend displayed a more uniform surface morphology than the $p$-PBDTPS−FTAZ:ITIC blend. As shown in Figure 3c,d, their bulk morphologies showed a fibril-like phase separation. It was conducive to create a fine channel for exciton diffusion and charge transport, affording large $J_{SC}$ values.

The charge carrier mobilities of the blend films were measured by means of space-charge-limited current, and the corresponding $J$−$V$ cures are displayed in Figure S6. Hole mobilities of $1.15 \times 10^{-4}$ and $4.16 \times 10^{-4}$ cm$^2$/(V s) were respectively observed for the blend films of $p$- and $m$-PBDTPS−FTAZ:ITIC. Additionally, electron mobilities of $3.93 \times 10^{-4}$ and $3.16 \times 10^{-4}$ cm$^2$/(V s) were respectively observed for the blend films of $p$- and $m$-PBDTPS−FTAZ:ITIC. Furthermore, ratios of the electron to hole mobilities ($\mu_e/\mu_h$) were calculated for both blend films according to their charge mobility values, which are 0.76 for $m$-PBDTPS−FTAZ:ITIC and 3.42 for $p$-PBDTPS−FTAZ:ITIC. Therefore, both polymers present decent electron

Table 2. Performance Parameters of Optimal Devices Based on the Two Polymers[a]

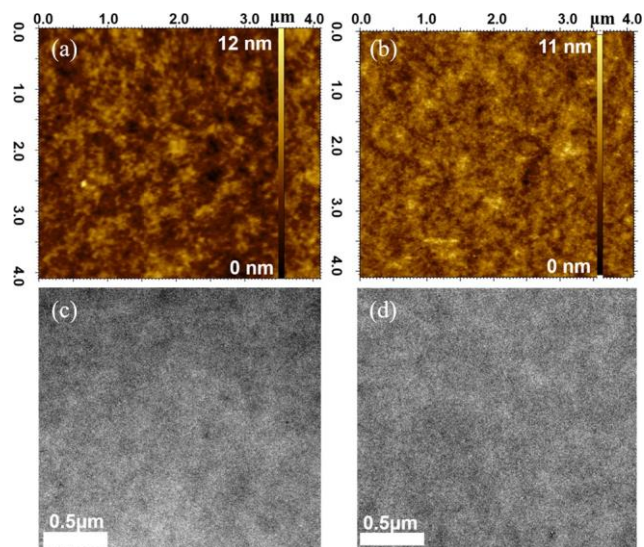| device | $V_{OC}$ (V) | $J_{SC}$ (mA/cm$^2$) | FF (%) | PCE (%) |
|---|---|---|---|---|
| *p*-PBDTPS−FTAZ:ITIC | 0.89 (0.88 ± 0.01) | 18.12 (17.91 ± 0.32) | 67.37 (66.11 ± 1.51) | 10.86 (10.54 ± 0.31) |
| *m*-PBDTPS−FTAZ:ITIC | 0.95 (0.95 ± 0.01) | 18.76 (18.02 ± 0.53) | 73.85 (71.53 ± 2.1) | 13.16 (13.01 ± 0.22) |

[a]Average PCE is calculated from 20 cells.



Figure 3. (a) Atomic force microscope (AFM) height image and (c) transmission electron microscope (TEM) image of the *p*-PBDTPS−FTAZ:ITIC blend film; (b) AFM height image and (d) TEM image of the *m*-PBDTPS−FTAZ:ITIC film.

and hole mobilities with a good balance of $\mu_e/\mu_h$, which are beneficial for their high photovoltaic performance.

The molecular orientations in active layers were investigated deeply by employing grazing-incidence wide-angle X-ray scattering (GIWAXS). As shown in Figure 4c, there were obvious (100) diffraction peaks at 0.27 and 0.31 Å$^{-1}$ in the in-plane direction for *p*- and *m*-PBDTPS−FTAZ:ITIC, respectively. This can be assigned to the ordered polymer interchain stacking in active layers. The corresponding *d*-spacings were
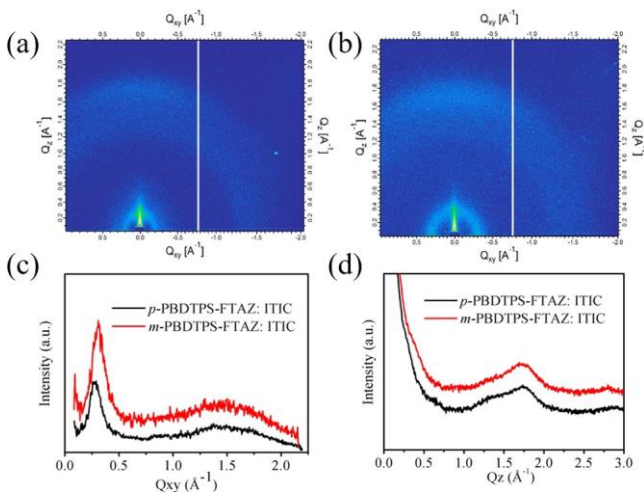
about 23.26 and 20.26 Å, respectively. The difference of lamellar distance may arise from the substituent on different sites on the phenyl group. Although the two blend films display a similar crystallinity here, the shorter corresponding *d*-spacing of the *m*-PBDTPS−FTAZ:ITIC blend suggests stronger intermolecular interactions than those of its *para*-isomer and therefore an improved charge transport (as the above-presented enlargement of four times of their hole mobility), which can also lead to a higher FF (from 67.37% for *para*- to 73.85% for *meta*-isomers).[44] Meanwhile, their AFM images and the RMS value of 0.99 nm for *m*-PBDTPS−FTAZ:ITIC have also confirmed a more uniform surface morphology than that of 1.09 nm for *p*-PBDTPS−FTAZ:ITIC, leading to the possible high mobility of the former than the latter. In addition, both the blend films exhibited a π−π stacking diffraction plotted at 1.74 Å$^{-1}$ as shown in Figure 4d, indicating that a face-on molecular orientation existed relative to the substrate. Meanwhile, the change of substituent sites had no obvious influence on the π−π stacking. Therefore, this work provided an effective way to modulate lamellar stacking while maintaining a π−π stacking feature.

The photocurrent density ($J_{ph}$) and the saturation current density ($J_{sat}$) were tested for exploring the exciton dissociation efficiencies ($P_{diss}$) via $J_{ph}/J_{sat}$, which could help understanding the photocurrent behaviors of OSCs. $J_{ph} = J_L − J_D$, where $J_D$ and $J_L$ are the current density in the dark and under illumination, respectively.[45] $J_{sat}$ values could be obtained by fitting the $J_{ph} − V_{eff}$ curves. Here, $V_{eff} = V_0 − V$, where $V_0$ and $V$ are the voltage at which $J_{ph} = 0$ and the applied voltage, respectively. The $J_{sat}$ values were about 19.5 and 19.8 mA/cm$^2$ for *p*- and *m*-PBDTPS−FTAZ OSCs, respectively, as displayed in Figure 5a. Corresponding $P_{diss}$ values of 93 and 95% were
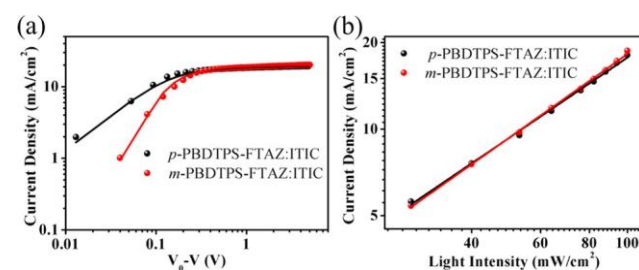


Figure 5. (a) $J_{ph} − V_{eff}$ curves and (b) $J_{SC}−P$ curves for *p*-PBDTPS−FTAZ- and *m*-PBDTPS−FTAZ-based OSCs.



Figure 4. GIWAXS scattering images for *p*-PBDTPS−FTAZ:ITIC (a) and *m*-PBDTPS−FTAZ:ITIC optimal blend films (b); and corresponding curves in the plane direction (c) and out-of-plane direction (d).

obtained for the former and latter, respectively. A high $P_{diss}$ indicated that charge carriers could be efficiently transported and collected by the corresponding electrodes. On the other hand, their charge recombination behavior was evaluated according to the dependence of $J_{SC}$ on the incident light power (P). $J_{SC}$ shows typically a power−law dependence on $P$ ($J_{SC} \propto P^\alpha$). The α values are about 0.92 and 0.96 for *p*-PBDTPS−FTAZ- and *m*-PBDTPS−FTAZ-based OSCs, respectively, as shown in Figure 5b. The α values of both devices are closer to

1.0, which indicated that bimolecular recombination was weak. Therefore, high FF values were achieved in both devices.

## CONCLUSIONS

In conclusion, the position of the alkylthio-substituted side chain has an impact on the HOMO energy level and molecular-packing distance, but no obvious effect on molecular crystallinity. Compared with $p$-PBDTPS−FTAZ, $m$-PBDTPS−FTAZ showed a slightly blue-shifted absorption and a lower HOMO energy value. When blending with ITIC, both of the polymers showed an obvious $\pi-\pi$ stacking, and $m$-PBDTPS−FTAZ showed a more uniform morphology than $p$-PBDTPS−FTAZ. Therefore, a promising PCE of 13.16% was achieved for $m$-PBDTPS−FTAZ:ITIC devices with a high $V_{OC}$ of 0.95 V, which was superior to that of $p$-PBDTPS−FTAZ. This work reported that $m$-BDTPS could be an effective donor unit to construct high-performance polymer donors with an appropriate acceptor unit to obtain both a higher $V_{OC}$ and larger $J_{SC}$.

## EXPERIMENTAL SECTION

Organic solar cells were prepared with a typical structure of ITO/PEDOT:PSS/polymer:ITIC/PFN-Br/Al. The patterned ITO glass with a sheet resistance of 15 $\Omega$/square was precleaned in an ultrasonic bath of acetone and isopropyl alcohol and then treated using an ultraviolet−ozone chamber for 6 min. Then, a 30 nm thick PEDOT:PSS layer was spin-coated onto the ITO glass and baked at 150 °C for 15 min. The mixed solutions of polymer and ITIC in $o$-DCB were stirred all night and then spin-coated on the PEDOT:PSS layer to prepare the light absorption layer with a thickness of 100−150 nm. A Veeco Dektak 150 profilometer was used to measure the thickness of the light absorption layer. The electron transport layer was prepared by spin-coating the PFN-Br solution (in $CH_3OH$). Finally, the metal electrode Al with a thickness of about 100 nm was thermally evaporated under about $4 \times 10^{-4}$ Pa and the device area was 0.1 cm$^2$ as defined by a shadow mask.

## ASSOCIATED CONTENT

### ✱ Supporting Information

The Supporting Information is available free of charge on the ACS Publications website at DOI: 10.1021/acsami.9b07112.

Device preparations, $J−V$ curves under different conditions, CV and TGA curves of two polymers, and DFT results (PDF)

## AUTHOR INFORMATION

### Corresponding Authors
*E-mail: zzh@qdu.edu.cn (Z.Z.).
*E-mail: yu@bio.aau.dk (D.Y.).
*E-mail: ergang@chalmers.se (E.W.).
*E-mail: yangrq@qibebt.ac.cn (R.Y.).
### ORCID
Weichao Chen: 0000-0002-7568-5820
Yonghai Li: 0000-0002-5748-0258
Ergang Wang: 0000-0002-4942-3771
Renqiang Yang: 0000-0001-6794-7416
### Author Contributions
#W.C. and G.H. contributed equally to this work.

### Author Contributions
The manuscript was written through contributions of all authors. All authors have given approval to the final version of the manuscript.

### Notes
The authors declare no competing financial interest.

## REFERENCES

(1) He, Z.; Zhong, C.; Su, S.; Xu, M.; Wu, H.; Cao, Y. Enhanced Power-Conversion Efficiency in Polymer Solar Cells Using an Inverted Device Structure. *Nat. Photonics* 2012, *6*, 591−595.

(2) Li, Y. Molecular Design of Photovoltaic Materials for Polymer Solar Cells: Toward Suitable Electronic Energy Levels and Broad Absorption. *Acc. Chem. Res.* 2012, *45*, 723−733.

(3) He, Z.; Xiao, B.; Liu, F.; Wu, H.; Yang, Y.; Xiao, S.; Wang, C.; Russell, T. P.; Cao, Y. Single-Junction Polymer Solar Cells with High Efficiency and Photovoltage. *Nat. Photonics* 2015, *9*, 174−179.

(4) Wu, J.-S.; Cheng, S.-W.; Cheng, Y.-J.; Hsu, C.-S. Donor-Acceptor Conjugated Polymers based on Multifused Ladder-Type Arenes for Organic Solar Cells. *Chem. Soc. Rev.* 2015, *44*, 1113−1154.

(5) Meng, D.; Sun, D.; Zhong, C.; Liu, T.; Fan, B.; Huo, L.; Li, Y.; Jiang, W.; Choi, H.; Kim, T.; Kim, J. Y.; Sun, Y.; Wang, Z.; Heeger, A. J. High-Performance Solution-Processed Non-Fullerene Organic Solar Cells Based on Selenophene-Containing Perylene Bisimide Acceptor. *J. Am. Chem. Soc.* 2016, *138*, 375−380.

(6) Meng, L.; Zhang, Y.; Wan, X.; Li, C.; Zhang, X.; Wang, Y.; Ke, X.; Xiao, Z.; Ding, L.; Xia, R.; Yip, H. L.; Cao, Y.; Chen, Y. Organic and Solution-Processed Tandem Solar Cells with 17.3% Efficiency. *Science* 2018, *361*, 1094−1098.

(7) Zhang, H.; Yao, H.; Hou, J.; Zhu, J.; Zhang, J.; Li, W.; Yu, R.; Gao, B.; Zhang, S.; Hou, J. Over 14% Efficiency in Organic Solar Cells Enabled by Chlorinated Nonfullerene Small-Molecule Acceptors. *Adv. Mater.* 2018, *30*, No. 1800613.

(8) Yuan, J.; Zhang, Y.; Zhou, L.; Zhang, G.; Yip, H.-L.; Lau, T.-K.; Lu, X.; Zhu, C.; Peng, H.; Johnson, P. A.; Leclerc, M.; Cao, Y.; Ulanski, J.; Li, Y.; Zou, Y. Single-Junction Organic Solar Cell with over 15% Efficiency Using Fused-Ring Acceptor with Electron-Deficient Core. *Joule* 2019, *3*, 1140−1151.

(9) Fan, B.; Zhang, D.; Li, M.; Zhong, W.; Zeng, Z.; Ying, L.; Huang, F.; Cao, Y. Achieving over 16% Efficiency for Single-Junction Organic Solar Cells. *Sci. China: Chem.* 2019, *6*, 746−752.

(10) Li, H.; Xiao, Z.; Ding, L. M.; Wang, J. Z. Thermostable Single-Junction Organic Solar Cells with a Power Conversion Efficiency of 14.62%. *Sci. Bull.* 2018, *63*, 340−342.

(11) Li, X.; Huang, G.; Zheng, N.; Li, Y.; Kang, X.; Qiao, S.; Jiang, H.; Chen, W.; Yang, R. High-Efficiency Polymer Solar Cells Over 13.9% With a High $V_{OC}$ Beyond 1.0 V by Synergistic Effect of Fluorine and Sulfur. *Sol. RRL* 2019, *3*, No. 1900005.

(12) Zhang, S.; Qin, Y.; Zhu, J.; Hou, J. Over 14% Efficiency in Polymer Solar Cells Enabled by a Chlorinated Polymer Donor. *Adv. Mater.* 2018, *30*, No. 1800868.

(13) Li, J.; Wang, Y.; Liang, Z.; Wang, N.; Tong, J.; Yang, C.; Bao, X.; Xia, Y. Enhanced Organic Photovoltaic Performance through Modulating Vertical Composition Distribution and Promoting Crystallinity of the Photoactive Layer by Diphenyl Sulfide Additives. *ACS Appl Mater Interfaces* 2019, *11*, 7022−7029.

(14) Huang, G.; Zhang, J.; Uranbileg, N.; Chen, W.; Jiang, H.; Tan, H.; Zhu, W.; Yang, R. Significantly Enhancing the Efficiency of a New Light-Harvesting Polymer with Alkylthio naphthyl Substituents Compared to Their Alkoxyl Analogs. *Adv. Energy Mater.* 2018, *8*, No. 1702489.

(15) Fan, B.; Du, X.; Liu, F.; Zhong, W.; Ying, L.; Xie, R.; Tang, X.; An, K.; Xin, J.; Li, N.; Ma, W.; Brabec, C. J.; Huang, F.; Cao, Y. Fine-Tuning of the Chemical Structure of Photoactive Materials for Highly Efficient Organic Photovoltaics. *Nat. Energy* 2018, *3*, 1051−1058.

(16) Wang, J.-L.; Zhang, H.-J.; Liu, S.; Liu, K.-K.; Liu, F.; Wu, H.-B.; Cao, Y. Branched 2-Ethylhexyl Substituted Indacenodithieno[3,2-b]Thiophene Core Enabling Wide-Bandgap Small Molecule for Fullerene-Based Organic Solar Cells with 9.15% Efficiency: Effect of Length and Position of Fused Polycyclic Aromatic Units. *Sol. RRL* 2018, *2*, No. 1800108.

(17) Jiang, H.; Li, X.; Liang, Z.; Huang, G.; Chen, W.; Zheng, N.; Yang, R. Employing Structurally Similar Acceptors as Crystalline Modulators to Construct High Efficiency Ternary Organic Solar Cells. *J. Mater. Chem. A* 2019, *7*, 7760−7765.

(18) Chen, W.; Huang, G.; Li, X.; Wang, H.; Li, Y.; Jiang, H.; Zheng, N.; Yang, R. Side-Chain-Promoted Benzodithiophene-based Conjugated Polymers toward Striking Enhancement of Photovoltaic Properties for Polymer Solar Cells. *ACS Appl. Mater. Interfaces* 2018, *10*, 42747−42755.

(19) Chen, W.; Shen, W.; Wang, H.; Liu, F.; Duan, L.; Xu, X.; Zhu, D.; Qiu, M.; Wang, E.; Yang, R. Enhanced Efficiency of Polymer Solar Cells by Improving Molecular Aggregation and Broadening the Absorption Spectra. *Dyes Pigm.* 2019, *166*, 42−48.

(20) Li, S.; Ye, L.; Zhao, W.; Yan, H.; Yang, B.; Liu, D.; Li, W.; Ade, H.; Hou, J. A Wide Band Gap Polymer with a Deep Highest Occupied Molecular Orbital Level Enables 14.2% Efficiency in Polymer Solar Cells. *J. Am. Chem. Soc.* 2018, *140*, 7159−7167.

(21) Xu, X.; Li, Z.; Wang, Z.; Li, K.; Feng, K.; Peng, Q. 10.20% Efficiency Polymer Solar Cells via employing Bilaterally Hole-Cascade Diazaphenanthrobisthiadiazole Polymer Donors and Electron-Cascade Indene-C70 Bisadduct Acceptor. *Nano Energy* 2016, *25*, 170−183.

(22) Xu, Z.; Fan, Q. P.; Meng, X. Y.; Guo, X.; Su, W. Y.; Ma, W.; Zhang, M. J.; Li, Y. F. Selenium-Containing Medium Bandgap Copolymer for Bulk Heterojunction Polymer Solar Cells with High Efficiency of 9.8%. *Chem. Mater.* 2017, *29*, 4811−4818.

(23) Zhang, M.; Guo, X.; Ma, W.; Ade, H.; Hou, J. A Polythiophene Derivative with Superior Properties for Practical Application in Polymer Solar Cells. *Adv. Mater.* 2014, *26*, 5880−5885.

(24) Su, W. Y.; Fan, Q. P.; Guo, X.; Meng, X. Y.; Bi, Z. Z.; Ma, W.; Zhang, M. J.; Li, Y. F. Two Compatible Nonfullerene Acceptors with Similar Structures as Alloy for Efficient Ternary Polymer Solar Cells. *Nano Energy* 2017, *38*, 510−517.

(25) Liao, X. F.; Yao, Z. Y.; Gao, K.; Shi, X. L.; Zuo, L. J.; Zhu, Z. L.; Chen, L.; Liu, F.; Chen, Y. W.; Jen, A. K. Y. Mapping Nonfullerene Acceptors with a Novel Wide Bandgap Polymer for High Performance Polymer Solar Cells. *Adv. Energy Mater.* 2018, *8*, No. 1801214.

(26) An, Y. K.; Liao, X. F.; Chen, L.; Yin, J. P.; Ai, Q. Y.; Xie, Q.; Huang, B.; Liu, F.; Jen, A. K. Y.; Chen, Y. W. Nonhalogen Solvent-Processed Asymmetric Wide-Bandgap Polymers for Nonfullerene Organic Solar Cells with Over 10% Efficiency. *Adv. Funct. Mater.* 2018, *28*, No. 1706517.

(27) Cheng, Y.-J.; Yang, S.-H.; Hsu, C.-S. Synthesis of Conjugated Polymers for Organic Solar Cell Applications. *Chem. Rev.* 2009, *109*, 5868−5923.

(28) Lu, L.; Zheng, T.; Wu, Q.; Schneider, A. M.; Zhao, D.; Yu, L. Recent Advances in Bulk Heterojunction Polymer Solar Cells. *Chem. Rev.* 2015, *115*, 12666−12731.

(29) Yao, H.; Ye, L.; Zhang, H.; Li, S.; Zhang, S.; Hou, J. Molecular Design of Benzodithiophene-Based Organic Photovoltaic Materials. *Chem. Rev.* 2016, *116*, 7397−7457.

(30) Li, J.; Liang, Z.; Wang, Y.; Li, H.; Tong, J.; Bao, X.; Xia, Y. Enhanced Efficiency of Polymer Solar Cells through Synergistic Optimization of Mobility and Tuning Donor Alloys by Adding High-Mobility Conjugated Polymers. *J. Mater. Chem. C* 2018, *6*, 11015−11022.

(31) Kang, Q.; Ye, L.; Xu, B.; An, C.; Stuard, S. J.; Zhang, S.; Yao, H.; Ade, H.; Hou, J. A Printable Organic Cathode Interlayer Enables over 13% Efficiency for 1-cm² Organic Solar Cells. *Joule* 2018, *3*, 227−239.

(32) Liang, Z.; Tong, J.; Li, H.; Wang, Y.; Wang, N.; Li, J.; Yang, C.; Xia, Y. The Comprehensive Utilization of the Synergistic Effect of Fullerene and Non-Fullerene Acceptors to Achieve Highly Efficient Polymer Solar Cells. *J. Mater. Chem. A* 2019, *7*, 15841−15850.

(33) Chakravarthi, N.; Gunasekar, K.; Kranthiraja, K.; Kim, T.; Cho, W.; Kim, C. S.; Kim, D.-H.; Song, M.; Jin, S.-H. The Effect of with/without Resonance-Mediated Interactions on the Organic Solar Cell Performance of New 2D π-Conjugated Polymers. *Polym. Chem.* 2015, *6*, 7149−7159.

(34) Gong, X.; Li, G.; Li, C.; Zhang, J.; Bo, Z. Benzothiadiazole based Conjugated Polymers for High Performance Polymer Solar Cells. *J. Mater. Chem. A* 2015, *3*, 20195−20200.

(35) Dou, L.; Gao, J.; Richard, E.; You, J.; Chen, C.-C.; Cha, K. C.; He, Y.; Li, G.; Yang, Y. Systematic Investigation of Benzodithiophene- and Diketopyrrolopyrrole-Based Low-Bandgap Polymers Designed for Single Junction and Tandem Polymer Solar Cells. *J. Am. Chem. Soc.* 2012, *134*, 10071−10079.

(36) Lu, H.; Zhang, J.; Chen, J.; Liu, Q.; Gong, X.; Feng, S.; Xu, X.; Ma, W.; Bo, Z. Ternary-Blend Polymer Solar Cells Combining Fullerene and Nonfullerene Acceptors to Synergistically Boost the Photovoltaic Performance. *Adv. Mater.* 2016, *28*, 9559−9566.

(37) Chen, W.; Jiang, H.; Huang, G.; Zhang, J.; Cai, M.; Wan, X.; Yang, R. High-Efficiency Ternary Polymer Solar Cells Based on Intense FRET Energy Transfer Process. *Sol. RRL* 2018, *2*, No. 1800101.

(38) Liu, T.; Huo, L.; Chandrabose, S.; Chen, K.; Han, G.; Qi, F.; Meng, X.; Xie, D.; Ma, W.; Yi, Y.; Hodgkiss, J. M.; Liu, F.; Wang, J.; Yang, C.; Sun, Y. Optimized Fibril Network Morphology by Precise Side-Chain Engineering to Achieve High-Performance Bulk-Heterojunction Organic Solar Cells. *Adv. Mater.* 2018, *30*, No. 1707353.

(39) Weng, K.; Xue, X.; Qi, F.; Zhang, Y.; Huo, L.; Zhang, J.; Wei, D.; Wan, M.; Sun, Y. Synergistic Effects of Fluorination and Alkylthiolation on the Photovoltaic Performance of the Poly-(benzodithiophene-benzothiadiazole) Copolymers. *ACS Appl. Energy Mater.* 2018, *1*, 4686−4694.

(40) Cui, C.; Wong, W.-Y.; Li, Y. Improvement of Open-Circuit Voltage and Photovoltaic Properties of 2D-Conjugated Polymers by Alkylthio Substitution. *Energy Environ. Sci.* 2014, *7*, 2276−2284.

(41) Aldrich, T. J.; Leonardi, M. J.; Dudnik, A. S.; Eastham, N. D.; Harutyunyan, B.; Fauvell, T. J.; Manley, E. F.; Zhou, N. J.; Butler, M. R.; Harschneck, T.; Ratner, M. A.; Chen, L. X.; Bedzyk, M. J.; Chang, R. P. H.; Melkonyan, F. S.; Facchetti, A.; Marks, T. J. Enhanced Fill Factor through Chalcogen Side Chain Manipulation in Small-Molecule Photovoltaics. *ACS Energy Lett.* 2017, *2*, 2415−2421.

(42) Garcia-Belmonte, G.; Gurrero, A.; Bisquert, J. Elucidating Operating Modes of Bulk-Heterojunction Solar Cells from Impedance Spectroscopy Analysis. *J. Phys. Chem. Lett.* 2013, *4*, 877−886.

(43) Boix, P. P.; Gurrero, A.; Marchesi, L. F.; Garcia-Belmonte, G.; Bisquert, J. Current-Voltage Characteristics of Bulk Heterojunction Organic Solar Cells: Connection Between Light and Dark Curves. *Adv. Energy Mater.* 2011, *1*, 1073−1078.

(44) Yao, Z.; Liao, X.; Gao, K.; Lin, F.; Xu, X.; Shi, X.; Zuo, L.; Liu, F.; Chen, Y.; Jen, A. K.-Y. Dithienopicenocarbazole-Based Acceptors for Efficient Organic Solar Cells with Optoelectronic Response Over 1000 nm and an Extremely Low Energy Loss. *J. Am. Chem. Soc.* 2018, *6*, 2054−2057.

(45) Wu, J.-L.; Chen, F.-C.; Hsiao, Y.-S.; Chien, F.-C.; Chen, P.; Kuo, C.-H.; Huang, M. H.; Hsu, C.-S. Surface Plasmonic Effects of Metallic Nanoparticles on the Performance of Polymer Bulk Heterojunction Solar Cells. *ACS Nano* 2011, *5*, 959−967.